Proceedings of the Korean Nuclear Society Spring Meeting
Cheju, Korea, May 2001

Experimental and Analytical Study on the Simulation of Pool Boiling CHF Based on Macrolayer Dryout Model

Yong-Hoon Jeong, Won-Pil Baek* and Soon Heung Chang

Department of Nuclear Engineering
Korea Advanced Institute of Science and Technology
* Korea Atomic Energy Research Institute

ABSTRACT

This paper presents a non-heating experimental- and analytical-method which simulates the critical heat flux (CHF) phenomenon in pool boiling. With providing controlled air flow through the holes on a plate submerged in a pool of water, the liquid sublayer (macrolayer) thickness and bubble departure frequency have been successfully measured by a conductance probe. The CHF is reasonably predicted by applying the measured parameters to a liquid macrolayer dryout model. The measured trends of the macrolayer thickness and bubble departure frequency with air mass flux are also consistent with the present understanding. On the other side, a simple analytical model in which bubble growth is simulated as a growth of spherical bubble is developed, and several parametric effects are studied. The general trends well agree with the experimental results and general understandings. Overall, the non-heating method would be useful to investigate the various parametric effects on pool and flow boiling CHF, with avoiding the difficulty in heating and large electric power requirement even for complex geometry.

1. Introduction

The critical heat flux (CHF) is an important thermal-hydraulic phenomenon which should be considered in designing and operating various heat transfer units including nuclear reactors, fossil-fueled boilers, electronic chips, etc. A significant amount of work has been performed over the last four decades to identify physical mechanisms leading to the CHF and to obtain reliable prediction models. However, understanding of the phenomenon is still insufficient in the aspects of detailed CHF mechanisms, effects of various parameters, prediction models applicable to wide range of conditions, etc.

One of the reasons for insufficient understanding is the difficulty in conducting CHF tests for complex geometry and/or high heat fluxes. Because the required heat flux should be supplied to test sections by direct or indirect electrical heating, the CHF of complex or large structures has not been investigated in detail. The non-heating simulation of CHF conditions is examined in this work to resolve this situation.

In developing the non-heating method for pool-boiling CHF, the liquid macrolayer (sublayer) dryout mechanism is assumed as the fundamental CHF mechanism. It has been suggested by several investigators as one of the most probable mechanisms of CHF occurrence. The model assumes periodic growth and

departure of a vapor clot on the heated surface and the existence of a liquid macrolayer between the heated surface and the vapor clot. The CHF is postulated to occur when the liquid in the macrolayer is depleted by evaporation during the growth of a large vapor clot. Therefore, the main parameters determining the CHF are the initial macrolayer thickness and bubble departure frequency. If we know these two values, we can calculate the corresponding CHF value.

Previous experiments by Gaetner [3], Katto and Yokota [8], and Bhat et al. [1] support the presence of the macrolayer under the vapor clot on the heater surface. Based on these observations, Haramura and Katto [5] suggested a macrolayer dryout model for prediction of pool-boiling CHF. They assume that the CHF occurs when the macrolayer is depleted before the detachment of overlying vapor bubble or bubbles:

$$q_{CHF} = d_l r_l h_{fg} (1 - A_v / A_w) f \qquad (1)$$

where f is the detachment frequency, d_l the initial macrolayer thickness, A_w the surface area of the heater, and A_v the total bottom area of vapor stems.

Several researchers have tried to measure the macrolayer thickness. Gaertner [3] observed macrolayers using an upward-facing horizontal disk of 50 mm diameter and discussed the relationship between the macrolayer thickness and the diameter of vapor stems in the macrolayer. After him, considerable measurements have been performed using conduction probes. In most experiments, the interface of macrolayer is determined by the position where the void fraction or bubble frequency changes drastically. From the heater wall to the the macrolayer boundary, void fraction and fluctuation frequency are nearly constant. Near the boundary, the void fraction increases drastically while the fluctuation frequency decreases drastically. From these evidences, they determined the macrolayer thickness.

In this study, the liquid macrolayer thickness and bubble departure frequency have been successfully measured by a conductance probe with providing controlled air flow through the holes on a plate submerged in a pool of water. The feasibility of the non-heating simulation is validated by applying the measured values to Eq. (1) and comparing the results with the well-known CHF values. The effects of the air mass flux on the macrolayer thickness and the bubble departure frequency are also compared with the previous understanding reported by others. This paper also discusses future possible applications of the non-heating method.

2. Experimental Method

Figure 1 shows a schematic of the experimental apparatus used in this study. The air-blowing surface is made of a copper plate of 50 mm where the diameter of the actual air-blowing area is varied from 25 to 40 mm. Nucleation sites are modelled by the small holes of 0.3 mm diameter, arranged with a pitch of 1 mm.

The correlations for active nucleation site density by Wang and Dhir [11] and Paul and Abdel-Khalik [9] were used to determine the number density of holes. Wang and Dihr [11] correlated their data of active nucleation site density as a function of the wall superheat and contact angle as follows:

$$N = 5 \times 10^{-27} (1 - \cos f) / d_c^6 \qquad (2)$$

where the cavity mouth diameter d_c is a function of the local superheating:

$$d_c = \frac{4\sigma T_{sat}}{\rho_g h_{fg} \Delta T} \quad (3)$$

For water under atmospheric pressure, the contact angle is about 85°, and the wall superheat is about 10~20°C. So, the active nucleation site density would be in the range of 60,000~4000,000 sites/m^2 or 250~2000 sites/m [2]. In other words, the pitch between active nucleation site would be 0.5~4 mm. On the other hand, Abdel-Khalik's correlation is given as follows [9]:

$$N = 1.207 \times 10^{-3} q + 15.74 \quad (4)$$

This represents the active nucleation site density of ~1585 sites/m for the CHF value of ~1300 kW/m^2 that is expected on the flat plate. The pitch between active nucleation sites would be ~0.6 mm. The pitch of 1 mm between drilled holes was determined based on the above considerations.

The heat flux condition was simulated by controlling the air-flow rate. Here, the heat flux q'' corresponds to the air-flow rate $\dot{V}$ as as follows:

$$q'' A = \dot{V} \rho h_{fg} \quad (5)$$

The void fraction was measured at various distances from the drilled plate by a conduction probe. The schematic of the conduction probe is shown in Fig. 2. The maximum diameter of probe tip is 0.075 mm, and the probe tip is canned by two of steel cans. The gaps between the tip and supporting cans are filled with epoxy and Teflon so that the tip and cans are electrically insulated. If the probe tip is contacted with water, the current path between the tip and outer can is established with generating the voltage signal of 3~5 V. If the tip is contacted with air bubbles, the current path becomes open and the voltage signal is dropped to a low value.

This voltage signals are gathered by using an A/D converter and a PC with an adequate data acquisition program (Fig. 1)..

For given air-blowing area and air flow rate, the void fraction distributions were measured at various distances between 0.02 to 30 mm from the drilled plate by changing the location of the conduction probe.

3. Experimental Results and Discussion

3.1 Measurement of the macrolayer thickness

The mesaured distribution of void fraction for the disk of 25 mm diameter (air- blowing area) is shown in Fig. 2. The void fraction (time-averaged resistance) is nearly constant and low near the wall, but sharply increases in the distance of 0.1~0.5 mm. The first transition points of the void fraction, which can be considered as the macrolayer thickness, are located in the range of 0.1~0.2 mm. Therefore the macrolayer thickness can be determined based on the void fraction distribution as in this work.

Several researchers have measured the macrolayer thickness in actual boiling boiling of water on horizontally upward-facing plates using various measuring device and suggested some experimental or theoretical correlations [3, 5, 7, 10]. Their correlations and the results of the present work are compared in Fig. 3. It is noted that non-boiling experimental results in this work agree reasonably well with previous heating experiments, in particular onsidering the difference between steam and air properties.

3.2 Measurement of the bubble departure frequency

The bubble departure frequency of flat disks has been measured by the conductance probe. It can be obtained by analyzing the signals from the conductance probe located at a sufficiently long distance from the air-blowing surface (x > 50 mm) as the vapor mushroom (clot) on the air-blowing surface is smaller than 50 mm. The measured bubble departure frequency according to various heat flux is shown in Fig. 4. Some of the measured frequencies were confirmed by the high-speed camera recordings.

Haramura and Katto [6] derived a correlation for the hovering period of vapor mass t_d as:

$$t_d = (3/4p)^{1/5}\{4[(11/16)r_l + r_v]/[g(r_l - r_v)]\}^{3/5} v_1^{1/5} \quad (6)$$

where v_1 is the vapor volume generation rate per unit heater area. Because the vapor volume generation rate is proportional to the applied heat flux, the hovering time increases with the increase in the heat flux. So, the bubble departure frequency is inversely proportional to the heat flux. This agrees with the measured results shown in Fig. 4.

3.3 Estimation of the critical heat flux

From the macrolayer thickness and bubble departure frequency, we can estimate the critical heat flux using Eq. (1), by replacing the term A_v / A_w as the measured void fraction a. Equation (1) can be rewriten as follows:

$$q_{CHF} = d_l r_l h_{fg} (1-a) f \quad (7)$$

The estimation of the CHF is illustrated in Fig. 5. Two types of predictions are presented in Fig. 5. The circle represents the prediction neglecting the effect of the void fraction in the liquid macrolayer; that is, the term $(1-a)$ is droped from Eq. (7). The triangle represents the prediction incorporating the void fraction according to Eq. (7).

As shown in Fig. 5., the difference between the predicted heat flux for dryout and the applied heat flux is reduced as heat flux is approaching to the CHF value. The CHF condition can be determined by the intersection points of two lines. It is noted that the CHF condition can be reasonably established by the present non-boiling tests but further improvements would be required from the quantitative viewpoint.

3.4 The role of non-heating experiments

Through this study, we can propose the non-heating experimental method as a useful alternative for investigating the CHF phenomenon. By the measuring void fraction, the macrolayer thickness and bubble departure frequency from non-heating tests, we can roughly determine the onset of CHF on actual boiling systems.

There is no doubt that the prototypic geometry and fluids should be used in CHF tests as far as possible. However, the prototypic test could be practically impossible in some cases of complex and large geometry, due to the difficulties in providing reasonable heat flux distributions. In this case, the non-heating experiment can be performed relatively easily to investigate various parametric trends as well as to get the rough estimate of the CHF.

The non-heating experiment with air can simulate only the saturated condition as air bubbles cannot be condensed in water. The difference of physical properties between steam and air also deteriorates the accuracy of the simulation. However, a steam-water system using a steam generator would allow more accurate simulation even for the subcooled condition.

By nature, active nucleation site density varies with the applied heat flux. But, in this methodology, the active nucleation site density is fixed. So, the measured characteristics may be valid at high heat flux conditions with the comparable nucleation site densities.

Despite these limitations, the non-heating method would be a powerful alternative in investigating the CHF mechanisms and parametric effects in both pool and flow boiling, considering the possibility of the relatively easy simulation tests.

4. Analytic Study

A distinctive characteristic of nucleate boiling is the generation of bubbles from preferential site randomly located on the heating surface. Increasing wall superheat activates more nucleation sites, resulting in a rapid increase in heat flux. With further increase in wall heat superheat, bubbles interfere with each other and begin to coalesce. Coalescence is primary caused by the interaction of bubbles from the same site at first, and then by bubble interactions at neighboring sites. The transition from the isolate bubble regime is accompanied not only by a change of bubble geometry, and therefore of flow pattern in the vicinity of the heating surface, but also the transition is associated with a change of heat transfer mechanisms. Thus, the active nucleation site density is defined as the number of active site per unit area of the heating surface, and the geometry of the bubble are the key factors characterizing nucleate boiling heat transfer.

4.1 Model Description

In this study, it is assumed that the geometry of growing bubbles is sphere or ellipsoid and they have same radius. In figure 6, a simple relation of adjacent bubbles is shown. In that figure, the pitch between active nucleation site is denoted as P, and radius of growing bubble is denoted as c. In previous experiments, it is observed that, the size of growing bubbles on every bubbling site(simulating nucleation site) are same. The reason why the volumes of growing bubbles are same is as follows. At first moment, all the bubbles start to grow at each site, and at next moment, the growing bubbles coalesced each other and form one big air (simulating vapor) mushroom. After that, the mushroom departs from blowing surface, and all sites are cleaned out by the sweeping force of mushroom. In this way, the bubbling is repeated and the resulted growing bubbles have same size.

Based on theses simple assumptions, the radius of growing bubble can be calculated using experimental parameters such as blowing rate, surface area, pitch and hovering time(bubble departure frequency).

$$r = \sqrt{c^2 - (c-y)^2} \ = \sqrt{y(2c-y)} \tag{8}$$

$$V_{bub} = \int_0^{t_0} \dot{I}_{bub} dt = \frac{\dot{I}_{tot} P^2}{A_{tot}} \Delta t = \frac{4}{3} p c^3 \tag{9}$$

$$c = \sqrt[3]{\frac{3\dot{J}_{tot} P^2 \Delta t}{4\rho A_{tot}}} \tag{10}$$

where $0 \le \Delta t \le \frac{1}{f}$

At any point, the cross section of unit cell can be achieved and it can be categorized into three cases. In case I, the radius of bubble is less then the half of pitch, and in case II, the radius is greater than the half of pitch and less than the half of diagonal. In case III, the radius is greater than the half of diagonal.

Case I: $(r < 0.5P)$ (Fig. 7)

In this case the area covered by bubble and void fraction of that cross section can be calculated as followings;

$$A_{bub} = \pi r^2 = \pi y(2c - y) \tag{11}$$

$$\alpha = \frac{A_{bub}}{P^2} \tag{12}$$

Case II: $(0.5P < r \le \frac{\sqrt{2}}{2} P)$ (Fig. 8)

In this case the area covered by bubble and void fraction of that cross section can be calculated as followings with some complexity;

$$A_{bub} = \frac{4\sin^{-1}(P/2r) - \pi}{4} y(2c - y) + 4\Pr\sqrt{1-(P/2r)^2} \tag{13}$$

$$\alpha = \frac{A_{bub}}{P^2} \tag{12}$$

Case III: $(\frac{\sqrt{2}}{2} P < r)$ (Fig. 9)

In this case the hole area covered by bubble and void fraction is equal to 1.0;

$$A_{bub} = P^2 \tag{14}$$

$$\alpha = \frac{A_{bub}}{P^2} = 1.0 \tag{12}$$

In this means, for time t, void fraction can be calculated from bottom of the bubble to top of the bubble. After that, by increasing time t from 0 to 1/f, $\alpha(t,z)$ can be achieved. And, by time-averaging $\alpha(t,z)$, $\overline{\alpha}(z)$ can be calculated.

4.2 Calculation Results and Discussion

For the horizontal flat plate, the time-averaged void fractions are calculated. From these calculations, the parametric effects of several parameters can be drawn and the feasibility of non-heating simulation can be supported. The detailed results are as followings;

Effect of Heat Flux

Parametric effect of heat flux is shown in figure 10 by fixing any other parameters. As shown in that figure, as heat flux increases, the void fraction shifted to left and the macrolayer thickness decreases. This trend is well agreed with previous works of other researchers. However, the effect of heat flux alone is not

much strong, because the increase of nucleation site density is not considered although the heat flux increases. Only, the blowing rate(vapor generation rate) increases as the heat flux increases.

Effect of Nucleation Site Density

Parametric effect of nucleation site density(pitch) is shown in figure 11. As shown in that figure, as nucleation site density increases, the void fraction curve shifted to left and resulted macrolayer thickness decreases. This trend is well agreed with general understandings also. In this case, the effect of nucleation site density is so strong, and the resulted macrolayer thickness varies much. Considering the effect of heat flux and nucleation site density, it can be drawn that the effect of heat flux is strong, because the increase of nucleation site density comes from increase of the heat flux.

Effect of Bubble Departure Frequency

Parametric effect of bubble departure frequency(departure frequency of large vapor mushroom) is shown in figure 12. As shown in that figure, as bubble departure frequency increases, the void fraction curve shifted to right and resulted macrolayer thickness increases. This trend is well agreed with general understandings also. As the frequency increases, more water can be introduced to blowing surface(heater surface) and the void fraction can be increased.

Effect of Bubble Shape

Parametric effect of bubble shape(ratio of horizontal radius to vertical radius) is shown in figure 13. As shown in that figure, the void fraction of long bubble is greater than the flat bubble, and the effect of bubble shape is strong as the effect of heat flux and nucleation site density.

As the large vapor mushroom departs from the heater surface, the space that the vapor takes is refilled with water. In this process, upward induced flow can be formed on heater surface, and by this effect, the bubble generated on the heater surface can be prolonged. Overall, the long bubble is formed by the induced flow generated by departing vapor mushroom.

In the experiment, bubble generating pitch is 1 mm, but not all the holes are active. According visual observation(photographic observation), active pitch is about 3 mm, and the horizontal to vertical ratio(e) is about 0.8. In figure 14, the most probable void fraction distribution is shown. In that case macrolayer thickness is about 100 μm, and this agrees well with the experimental result.

Simulation of Steam-Water System (Heating Experiment)

Using the active nucleation site density of Eq. (4) and bubble departure frequency of Eq. (6), the void fraction distribution on heating surface can be simulated. As increasing the applied heat flux on heating surface, the resulted void fraction distribution shifted to left and the macrolayer thickness decreases[Fig. 15]. And, the predicted macrolayer thickness is well agreed with the correlation of Haramura & Katto [Fig. 3]. The critical heat flux can be predicted by using the macrolayer thickness and bubble departure frequency. In this simulation, the pool boiling CHF of horizontal flat plate is about 1050 kW/m^2 [Fig. 16]. Although, it is somewhat under estimated value, it can show the feasibility of non-heating simulation method.

5. Conclusions

In this study, a series of non-heating experiments and analytical study have been conducted to model the CHF in pool-boiling systems. Through this study, the void fraction, macrolayer thickness and bubble departure frequency are measured and the feasibility of non-heating experiment is studied. And, the analytical study support the conducted experiments. Important findings from this study are summarized as follows:

a) The liquid macrolayer thickness and the bubble departure frequency on air-blowing are measured successfully on the drilled disks submerged in water pool where controlled air flow is provided through the holes.

b) The measured macrolayer thickness and bubble departure frequency are consistent with previous findings in actual boiling tests.

c) Application of the macrolayer dryout model with the measured values provides reasonable CHF values, confirming the usefulness of the non-heating simulation of the pool-boiling CHF.

d) According to the analytical modelling, the formation of macrolayer is mainly due to coalescence of adjacent bubbles. And, the parametric trends well agree with general understandings.

e) Through the analytical modelling, the calculated void fraction distribution well agrees with the experimental results, and this can support the feasibility of non-heating modelling of pool boiling CHF.

f) The predicted pool boiling CHF is about 1050 kW/m^2, and it is in the reasonable boundary.

g) The non-heating method with further improvement would be useful in investigating the fundamental mechanisms and parametric effects in both pool and flow boiling involving complex geometries.

Nomenclature

A_v	total bottom area of vapor stems	m^2
A_w	surface area of heater	m^2
d_c	cavity mouth diameter	m
f	detachment frequency	Hz
h_{fg}	heat of vaporization	J/kg-K
N	active nucleation density	sites/m^2 of sites/m
T_{sat}	saturation temperature	K
ΔT	wall super heat	K
q_{CHF}	critical heat flux	W/m^2
d_l	initial macrolayer thickness	m
f	contact angle between heater surface and bubble	-
r_g	vapor density	kg/m^3
r_l	liquid density	kg/m^3
Dr	density difference between liquid and gas	kg/m^3
s	surface tension	N/m

μ viscosity of liquid

Subscripts

f Liquid

g Vapor

References

[1] A.M. Bhat, R. Prakash, J.S. Saini, On the mechanism of macrolayer formation in nucleate boiling at high heat flux, Int. J. Heat Mass Transfer, 26 (1986) 735-740.

[2] J.G. Collier, L.R. Thome, Convective boiling and condensation, Clarendon Press, 3rd Edition (1994) 142.

[3] R.F. Gaertner, J.W. Westwater, Population of active sites in nucleate boiling heat transfer, Chem. Engrg Prog. Symp. Ser. 46 (1960) 39-48.

[4] R.F. Gaertner, Photographic study of nucleate boiling on a horizontal surface, ASME J. Heat Transfer 87 (1965) 17-29.

[5] Y. Haramura, Y. Katto, New hydrodynamic model for critical heat flux (CHF), Trans. JSME 49 (1986) 1919-1927.

[6] Y. Haramura, Y. Katto, A new hydrodynamic model of critical heat flux, applicable widely to both pool and forced convection boiling on submerged bodies in saturated liquids, Int. J. Mass Transfer 26 (1983) 389-399.

[7] Y. Iida, K. Kobayashi, An experimental investigation of the effect of subcooling on bubble growth and waiting time in nucleate boiling, ASME J. Heat Tansfer 107 (1970) 168-174.

[8] Y. Katto, Y. Yokoya, Mechanisms of burnout and transition boiling in pool boiling, Trans. JSME 37 (1971) 535-545.

[9] D.D. Paul, S.I. Adel-Khalik, A statistical analysis of saturated nucleate boiling along a heated wire, Int. J. Heat Mass Transfer 26 (1983) 509-519.

[10] M. Shoji, A study if steady transition boiling of water: experimental verification of macrolayer evaporation model, Proc. on the Engineering Foundation Conference on Pool and External Flow Boiling, Santa Barbara, California (1992) 237-242.

[11] C.H. Wang, V.K. Dhir, Effect of surface wettability on active nucleation site density during pool boiling of water on a vertical surface, J. Heat Transfer 115 (1993) 659-669.

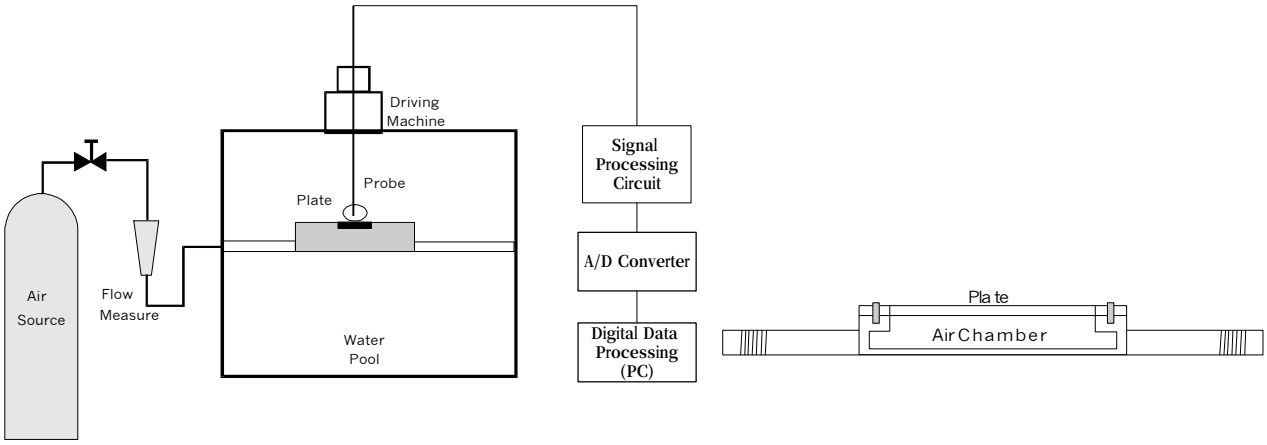

(a) Arrangement of apparatus (b) Cross section of test section

Fig. 1 Schematic diagram of the experimental apparatus

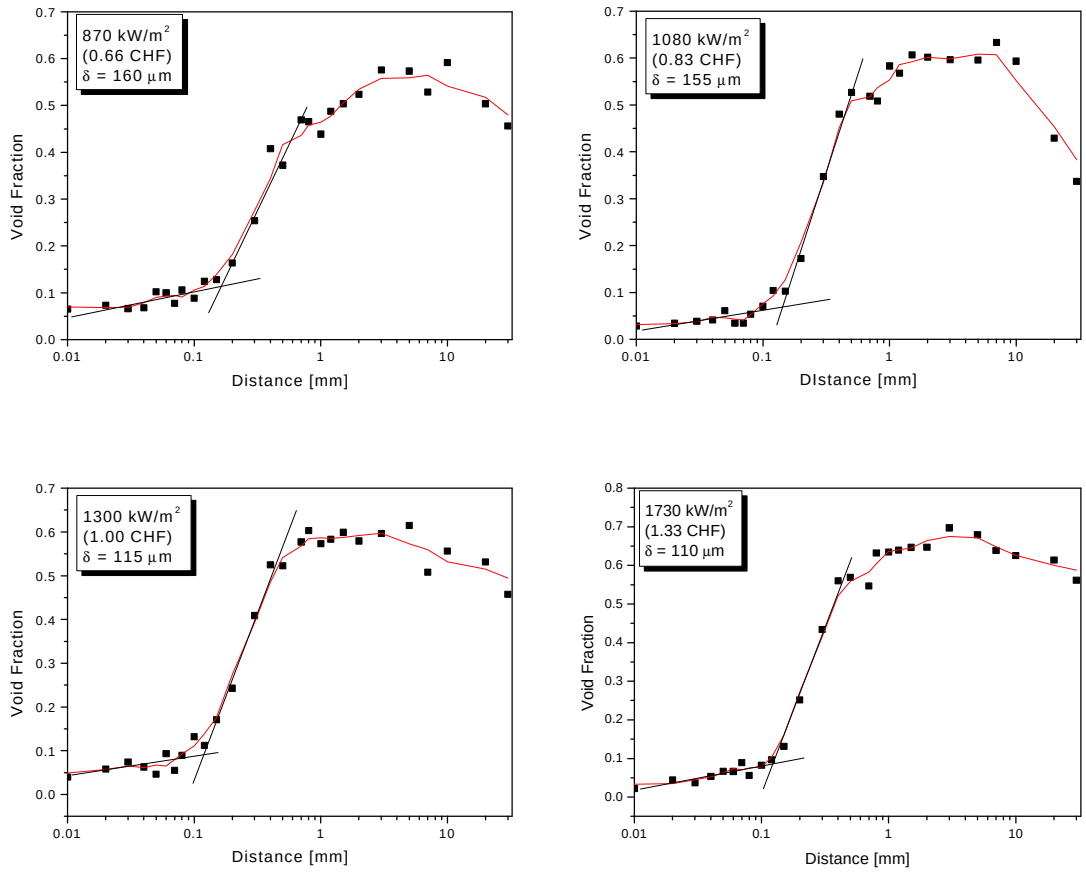

Fig. 2 Void fraction distribution (D=25 mm)

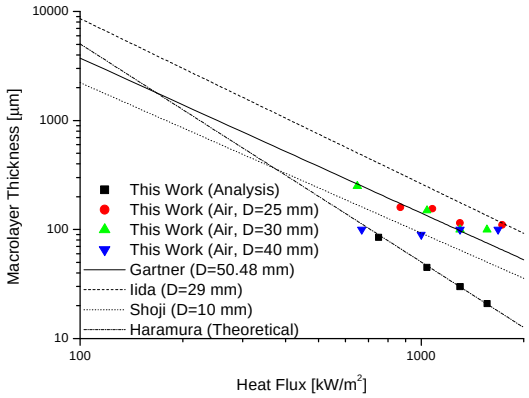

Fig. 3 Behavior of macrolayer thickness with heat flux

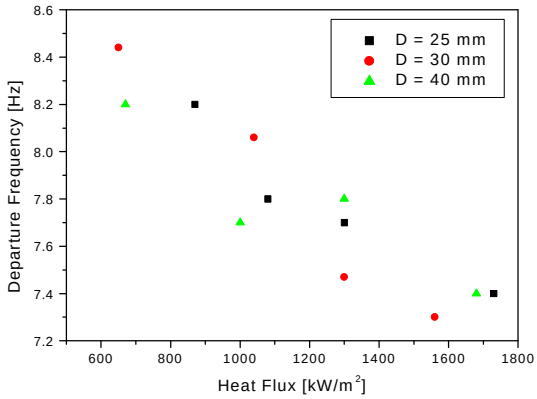

Fig. 4 Bubble departure frequency

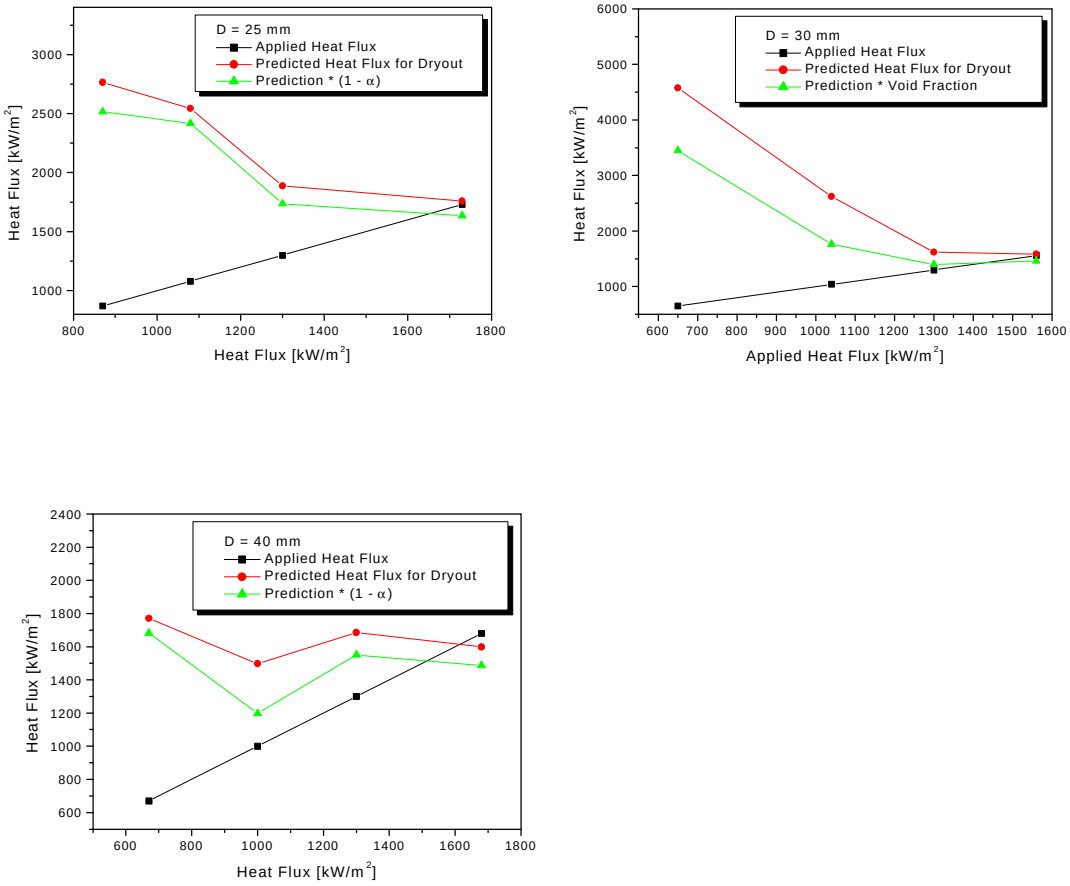

Fig. 5 CHF prediction using macroalyer thickness and bubble departure frequency

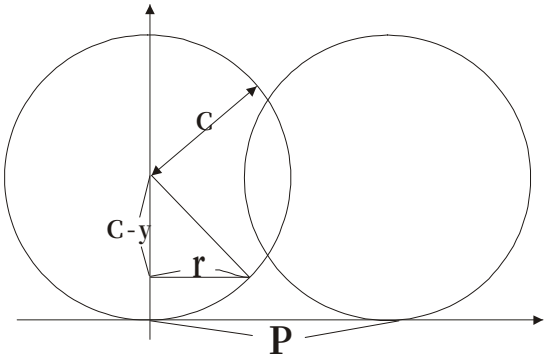

Fig. 6 Simple relationship between adjacent bubbles

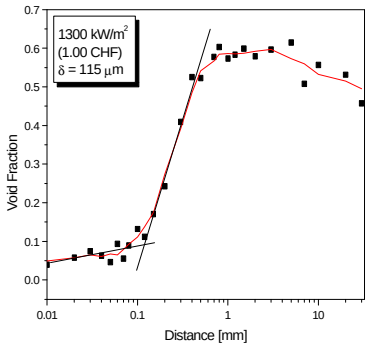

Fig. 7 Cross section of unit cell for case I

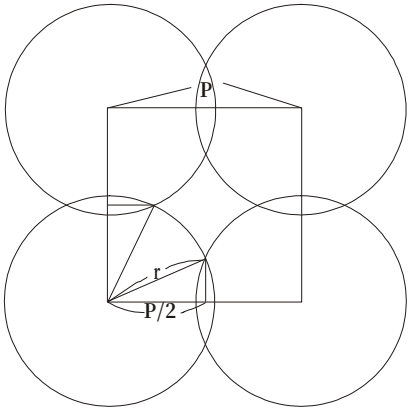

Fig. 8 Cross section of unit cell for case II

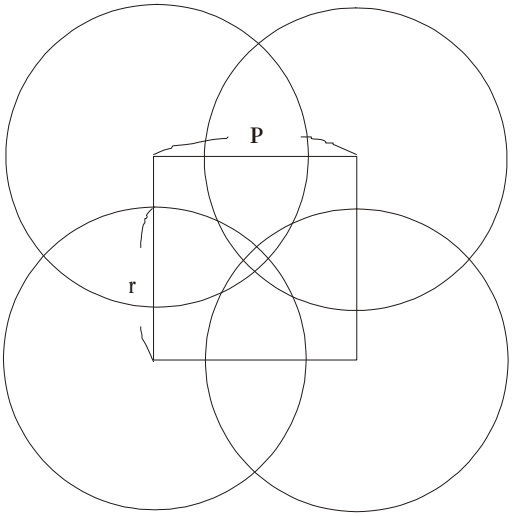

Fig. 9 Cross section of unit cell for case III

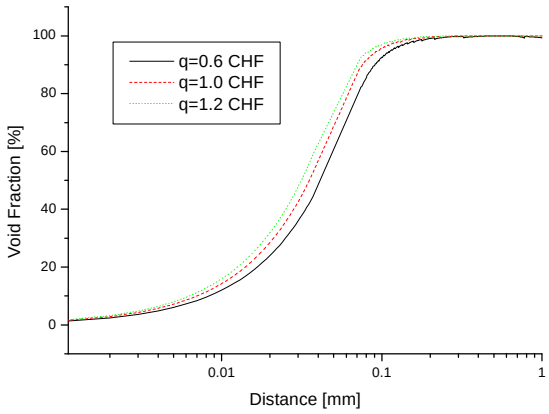

Fig. 10 Heat flux effect on void fraction distribution

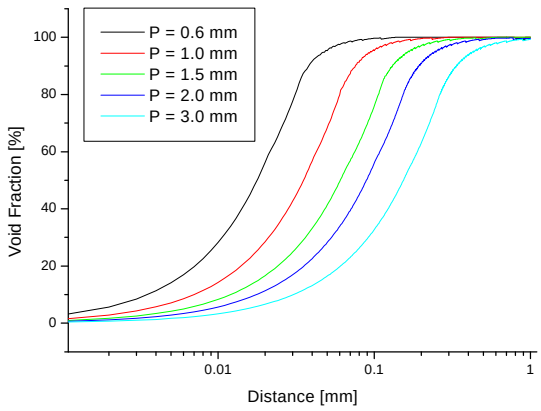

Fig. 11 Nucleation site density effect on void fraction distribution

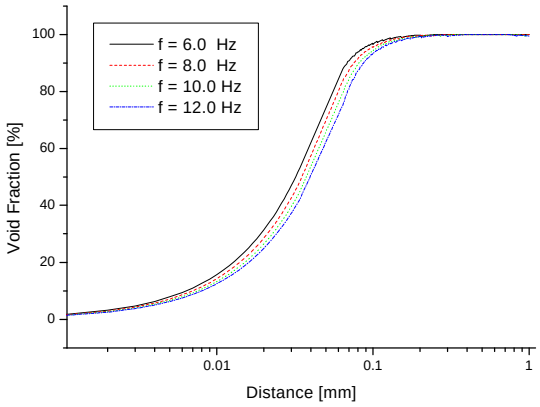

Fig. 12 Bubble departure frequency effect on void fraction distribution

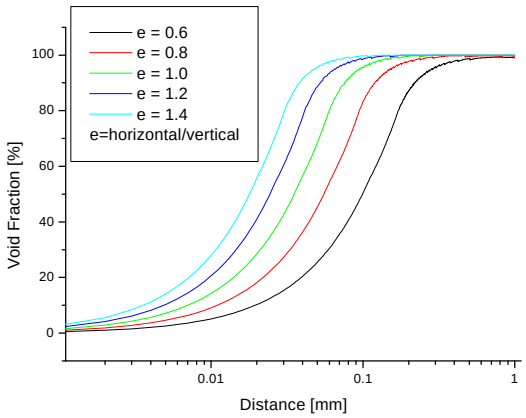

Fig. 13 Bubble shape effect on void fraction distribution

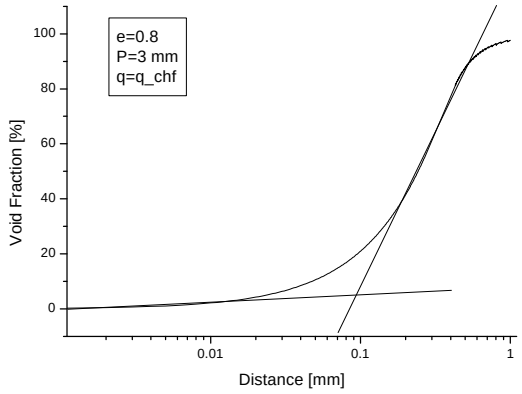

Fig. 14 Void fraction distribution (most probable configuration)

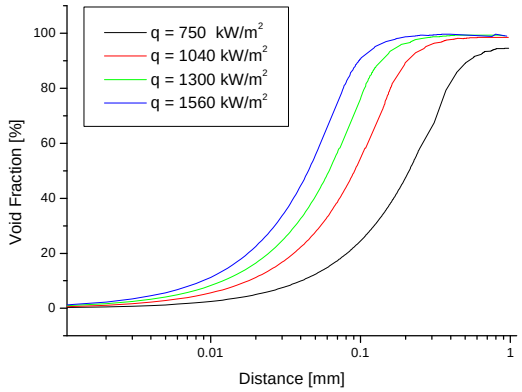

Fig. 15 Void fraction distribution (heating simulation)

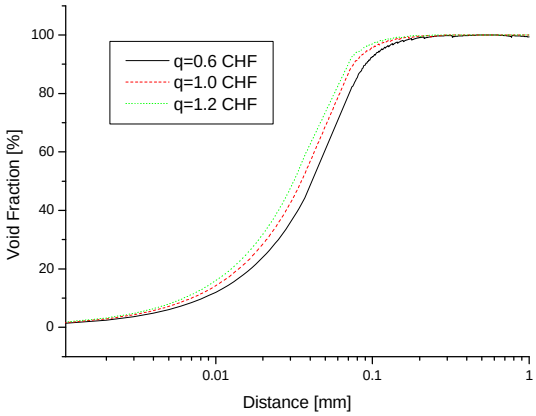

Fig. 16 Prediction of CHF (heating simulation)